RSC Advances

ROYAL SOCIETY OF CHEMISTRY

www.rsc.org/advances

The Table of Contents

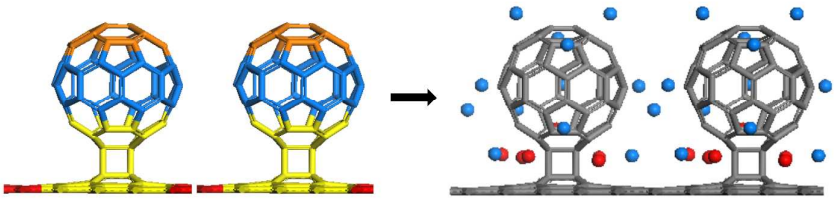

The adsorption mechanism of Li onto the graphene-C_{60} nanobud structure

Journal Name

RSCPublishing

ARTICLE

Li Adsorption on a Graphene–Fullerene Nanobud System: Density Functional Theory Approach

Cite this: DOI: 10.1039/x0xx00000x

Wonsang Koh,[a] Ji Hye Lee,[b] Seung Geol Lee,[*b] Ji Il Choi,[c] and Seung Soon Jang[*d]

Received 00th January 2012,
Accepted 00th January 2012

DOI: 10.1039/x0xx00000x

www.rsc.org/

In this study, we investigated the mechanisms of Li adsorption on a graphene-C_{60} nanobud system using density functional theory. Li adsorption on the hybrid system was enhanced compared to those in the case of pure graphene and C_{60}. The Li adsorption energies ranged from −1.784 to −2.346 eV for the adsorption of a single Li atom, and from −1.905 to −2.229 eV for the adsorption of two Li atoms. Furthermore, the adsorption energies were similar at most positions throughout the structure. The Li adsorption energy of an 18-Li adsorbed system was calculated to be −1.684 eV, which is significantly lower than the Li–Li binding energy (−1.030 eV). These results suggest that Li atoms will be adsorbed preferentially 1) between C_{60} and C_{60}, 2) between graphene and C_{60}, 3) on graphene, or 4) on C_{60}, rather than form Li clusters. As more Li atoms were adsorbed onto the graphene-C_{60} nanobud system because of its improved Li adsorption capability, the metallic character of the system was enhanced, which was confirmed via analysis of the band structure and electronic density of states.

Introduction

Currently, a variety of carbonaceous materials such as carbon nanotubes (CNTs), fullerene (C_{60}), and graphene are used as anodes in Li-ion battery applications. Among these diverse materials, great attention has been focused on graphene-based anodes because graphene possesses extraordinary optical, electrical, and mechanical properties as well as a large surface area. For example, although both graphite and graphene can adsorb Li, adsorption on graphite generates a LiC_6 form with a Li storage capacity of 372 $mAh \cdot g^{-1}$ owing to its tightly stacked layered structure,[1] whereas Li adsorption on graphene generates a LiC_3 form[2] with a Li storage capacity of 500–1100 $mAh \cdot g^{-1}$ because Li is stored on both sides of the graphene. To further increase Li adsorption capacities, both theoretical[3] and experimental[4] studies have been conducted for various graphene morphologies including powders, nanoribbons, and nanosheets. However, the enhancement of Li storage capacity using pure graphene-based materials is limited. Hence, some theoretical[5] and experimental[4b, 6] studies have attempted to investigate graphene-C_{60} hybridized structures because the Li storage capacity is enhanced with the addition of C_{60}. Wu et al.[5a] prepared two prototype graphene-C_{60} hybridized structures, called periodic graphene nanobuds (PGNBs), by covalently bonding C_{60} to the surface of graphene or fusing fragmented C_{60}s onto a graphene monolayer. They showed that the electronic properties of the PGNBs depend on the covalent bonding configuration between the C_{60} and graphene. Using density functional theory (DFT) calculations, Skardi et al.[5e] studied the characteristics of Li adsorption on graphene and PGNBs, in which a large-sized C_{60} fragment was fused with a defective graphene. They considered six possible adsorption sites for a Li atom on the PGNBs and calculated the binding energies. The results showed that the hollow site above the center of the hexagon ring of a PGNB is the most energetically stable with a binding energy of −2.58 eV owing to the significant charge transfer from the Li atom to the PGNB. This result emphasized that the electronic properties of the PGNB change following the adsorption of a Li atom, and demonstrated that a strong interaction exists between the Li atom and the PGNB surface. Hence, to develop functional energy storage devices, it is important to understand the electronic properties of the graphene-C_{60} nanobud structure in the presence of Li atoms.

In this study, we focused on a covalently bonded graphene-C_{60} nanobud system to investigate its capacity for the adsorption of single as well as multiple Li atoms. Graphene-C_{60} nanobuds are hybrid zero-dimensional and two-dimensional carbon materials with varied electronic and magnetic characteristics depending on the connection points of both the graphene and C_{60}.[5f] The graphene-C_{60} nanobud system utilizes C_{60} as the electron acceptor from Li and graphene as the charge transport channel throughout the electrode. Therefore, Li adsorption on the graphene-C_{60} electrode is expected to be more favorable than on a pure graphene-based electrode because of the higher electron affinity of C_{60}. We used the first-principles computational method DMol[3] from Accelrys[7] to investigate the electrochemical characteristics of the graphene-C_{60} nanobud system, such as its adsorption capabilities and charge transfer properties. We calculated the Li adsorption energy of the hybrid system and the accompanying changes in electronic properties such as band structure, density of states (DOS), and charge distribution as a function of Li adsorption using DFT. In addition, we studied the mechanism of Li adsorption in comparison with Li cluster formation by calculating Li

adsorption energies on various regions of the graphene-C_{60} nanobud structure.

Experimental

We used a generalized gradient approximation (GGA) of the Perdew-Burke-Ernzerhof (PBE) functional[8] with a double numerical basis set including d-polarization functions (DND) for all the DFT calculations. The PBE functional has been used to successfully describe the interactions between an adsorbate and various surfaces[9] including sp^2 carbon-based materials.[10] The DFT-D3 correction was incorporated into the PBE functional to handle dispersion interactions.[11] The unit cell dimensions of 12.3 Å × 12.3 Å × 35 Å were large enough to ensure that there was no direct interaction between the original structure and its self-image through the periodic boundary along the *c*-axis, with the *a*- and *b*-axis dimensions determined from the area of the graphene. The k-point sampling of the Brillouin zone was performed using the Monkhorst-Pack special k-point scheme with a 4 × 4 × 1 grid in order to determine the adsorption energy and other electronic properties such as band structure, DOS, and Mulliken charge distribution. The adsorption of Li was performed at the center of the hexagon sites ("center") in graphene and the pentagon/hexagon sites of C_{60} because these sites showed the most stable adsorption energies. The adsorption energies and electronic properties of the graphene-C_{60} nanobud system were compared with those of pure graphene and the C_{60} face-centered cubic (fcc) crystal structure with a (111) surface. The adsorption energy was defined per Li atom on graphene. We defined the adsorption energy per Li atom on the graphene-C_{60} nanobud system ($\Delta E_{adsorption}$) as:

$$\Delta E_{adsorption} = \frac{E[nLi + nanobud\ \ system] - (E[nanobud\ \ system] + n \times E[Li])}{n} \quad (1)$$

where n is the number of the Li atoms and $E[nLi + nanobud\ system]$, $E[nanobud\ system]$, and $E[Li]$ are the energies of the Li-adsorbed graphene-C_{60} system, the system without Li, and a single Li atom in a vacuum, respectively.

Results and discussion

Pure graphene-C_{60} nanobud system

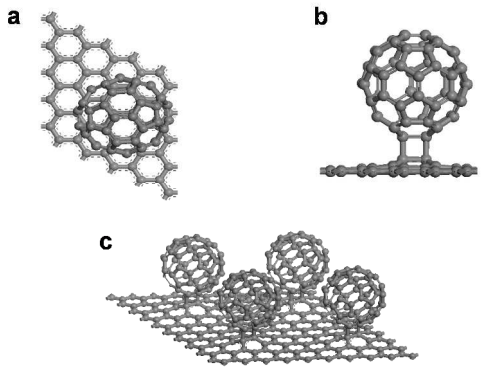

Fig. 1 The unit cell structure of the graphene-C_{60} nanobud system: (a) top, (b) side, and (c) expanded views. The cell parameters are $a = b = 12.3$ Å, $c = 35$ Å, $\alpha = \beta = 90°$, and $\gamma = 120°$

We fully optimized the geometry of the graphene-C_{60} nanobud system before we studied its Li adsorption capabilities. Fig. 1a–c shows the top, side, and expanded views of the structure. For this system, we considered two structures that connected the C–C bonds in graphene with the two possible C–C bonds in C_{60}: (i) a bond between two hexagonal faces (h) and (ii) a bond between a hexagonal (h) and pentagonal (p) face via [2+2] cycloaddition. Then, we calculated the binding energies ($E_{binding} = E_{nanobud} - E_{graphene} - E_{C60}$) of the hh and hp graphene-C_{60} structures. The binding energy, bond length, charge transfer from graphene to C_{60} through Mulliken analysis, and the band gap of each nanobud structure are summarized in Table 1.

Table 1 Binding energy, bond length, Mulliken charge distribution, and band gap of the graphene-C_{60} nanobud system

System	Binding energy (eV)	Bond length (Å)	Charges (e)		Band gap (eV)
			Graphene	C_{60}	
Graphene-C_{60} (hh)	2.632	1.637	0.059	-0.059	0
Graphene-C_{60} (hp)	3.319	1.652	0.103	-0.103	0.30

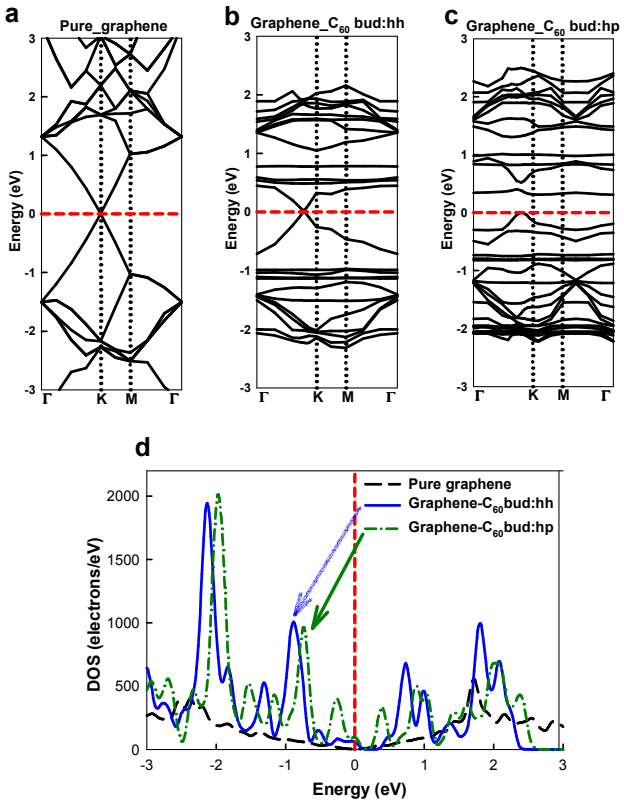

Fig. 2 Band structures of (a) pure graphene, (b) graphene-C_{60} nanobud:hh, and (c) graphene-C_{60} nanobud:hp systems (Γ = (0, 0, 0), K = (−1/3, 2/3, 0), and M = (0, 1/2, 0) in the Brillouin zone). (d) The density of states (DOS) of pure graphene, graphene-C_{60} nanobud:hh, and graphene-C_{60} nanobud:hp systems.

As shown in the table, the binding energy of the hh structure (2.632 eV) appears more favorable than that of the hp structure

(3.319 eV). However, to obtain the nanobud structures, extra energy was needed to form the covalent bonds via the sp^3 hybridization of carbon. A narrow band gap of 0.30 eV was developed between the orbitals of graphene and C_{60} in the middle of the hybridization when graphene was connected to the bond between the pentagonal and hexagonal sites of the C_{60}. The charge distribution of the system through Mulliken population analysis showed charge transfer from the graphene to C_{60} for all of the systems owing to the relatively strong electron affinity of C_{60}.

The band structures and DOS of pure graphene, pure C_{60}, and the graphene-C_{60} nanobud system are represented in Fig. 2. The graphene-C_{60} nanobud system has different characteristics than its components and shows a unique band structure because of the covalent bonds between graphene and C_{60}. The band structure also differs depending on the C–C bond position, which can be attributed to the π-bonds involved in the reaction. Hence, graphene-C_{60} nanobud:hh has no band gap, whereas graphene-C_{60} nanobud:hp has an indirect band gap (0.30 eV) owing to the different degree of π-bond character in these systems.

Adsorption of a single Li atom on the graphene-C_{60} nanobud system

We subsequently studied the adsorption of one Li atom on pure graphene, pure C_{60}, and at various positions in the hybrid nanobud system. For this evaluation, we chose the graphene-C_{60} nanobud:hh system because its formation requires less energy (2.632 eV) than the graphene-C_{60} nanobud:hp structure (3.319 eV) and because of its smaller band gap. Furthermore, we were interested in the electron conduction capabilities of these systems as electrodes. The Li atom was placed in the centers of hexagonal sites in graphene and pentagonal or hexagonal sites in C_{60} (which exhibit the most stable Li adsorption in C_{60}).[12] Regarding the stability of the graphene-C_{60} nanobud, we optimized the graphene-C_{60} nanobud:hh structure by varying distance from the optimized structure to obtain the energy barrier to dissociate the C_{60} from the graphene. As shown in Fig. 3, the relative energy is increased with increasing the distance, which is evidence that the optimized structure of the graphene-C_{60} nanobud is a meta-stable structure.

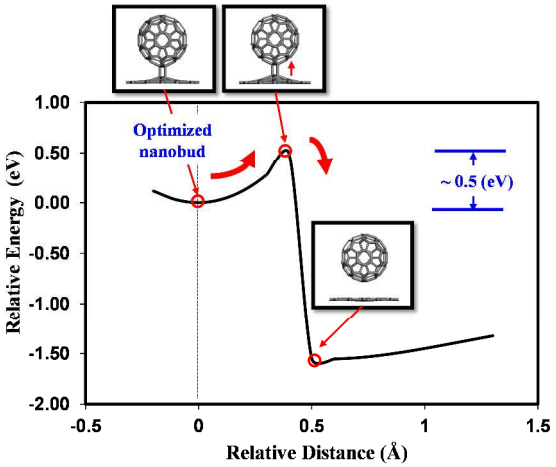

Fig. 3 The energy barrier from the graphene-C60 nanobud to the graphene-C60 system.

It is also found that, at 0.4-0.5 Å (relative distance from the optimized nanobud structure), the chemical bonds between C_{60} and neighbor carbons from graphene are break and the global minimum energy point is obtained. The energy barrier from the graphene-C_{60} nanobud to the graphene-C_{60} hybrid system is determined as ~ 0.50 eV, which confirms that the graphene-C_{60} nanobud is in a meta-stable state.

To describe the Li adsorption mechanism on the graphene-C_{60} nanobud system more systematically, we defined four distinct adsorption regions, as shown in Fig. 4a–d: (i) graphene side (region 1, red), (ii) between graphene and C_{60} (region 2, yellow), (iii) between C_{60}s (region 3, blue), and (iv) C_{60} side (region 4, orange). The Li atom is expected to interact with graphene alone in region 1 and with C_{60} alone in regions 3 and 4, whereas it can interact with both graphene and C_{60} simultaneously in region 2.

We placed one Li atom at various positions in each region of the graphene-C_{60} nanobud system, as shown in Fig. 4. The adsorption energies and charge distributions of the one-Li adsorption systems are summarized in Table 2. The adsorption of Li on the graphene side (−1.905 eV) was enhanced compared with that of pure graphene (−1.375 eV). This enhancement can possibly be explained by the charge distribution of the graphene-C_{60} nanobud system and the unit structure of the nanobud system. For example, in the absence of Li, a small degree of charge (|0.059|e) is transferred from graphene to C_{60}, making the graphene positively charged (Table 2). Thus, charge transfer from the adsorbed Li can occur to a greater extent in the graphene side region, contributing to its enhanced adsorption. At the same time, a Li atom in region 1 can still interact with C_{60} because of the planar structure of graphene and the size of the unit structure of the graphene-C_{60} nanobud system. We could confirm this interaction through the amount of charge transfer to C_{60} (−0.334e), which is comparable with that to graphene (−0.524e). Most of the Li atoms maintained their original position after optimization.

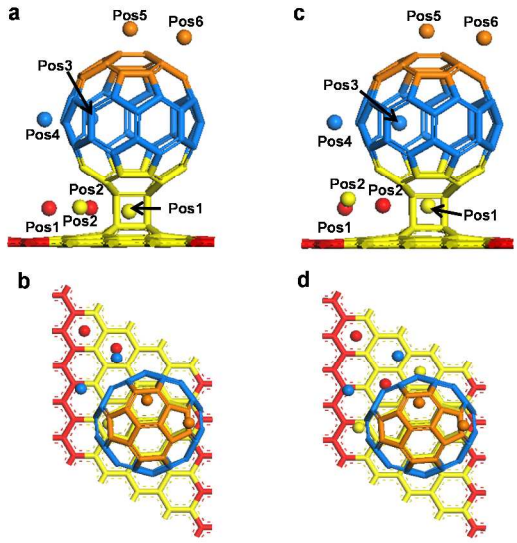

Fig. 4 Adsorption of one Li atom at various positions around the graphene-C_{60} nanobud system: (a) side and (b) top views of initial structure; (c) side and (d) top views of optimized structure. Region 1: red, region 2: yellow, region 3: blue, and region 4: orange.

Table 2 Adsorption energies and charge distributions (Mulliken charges) of one Li atom adsorbed on the graphene-C_{60} nanobud system

System	Adsorption Energy (eV)	Charge (e)		
		Li	graphene	C_{60}
graphene-C_{60} (hh)	N/A	N/A	0.059	−0.059
1 Li on graphene	−1.375 (−1.096[3b])	0.813	−0.813	N/A
1 Li on C_{60} (pentagon)	−1.838 (−1.820[13])	0.794	N/A	−0.794
Pos1@graphene (region1)	−1.905	0.858	−0.524	−0.334
Pos2@graphene (region1)	−2.346	0.863	−0.428	−0.435
Pos1@C_{60} (region2_hexa)	−2.345	0.871	−0.427	−0.444
Pos2@C_{60} (region2_penta)	−2.182	0.856	−0.477	−0.379
Pos3@C_{60} (region3_hexa)	−2.002	0.856	−0.028	−0.828
Pos4@C_{60} (region3_penta)	−2.158	0.865	−0.025	−0.840
Pos5@C_{60} (region4_hexa)	−1.784	0.800	−0.015	−0.785
Pos6@C_{60} (region4_penta)	−1.840	0.785	−0.011	−0.774

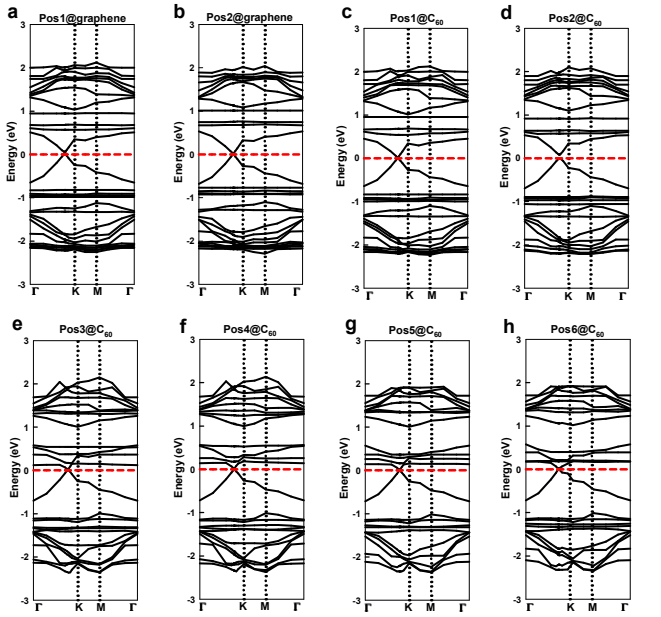

Fig. 5 The band structures for adsorption of one Li atom at various positions on the graphene-C_{60} nanobud system: (a) Pos1@graphene, (b) Pos2@graphene, (c) Pos1@C_{60}, (d) Pos2@C_{60}, (e) Pos3@C_{60}, (f) Pos4@C_{60}, (g) Pos5@C_{60}, and (h) Pos6@C_{60}.

However, the Li atom positioned near C_{60} (Pos2@graphene) clearly moves closer to C_{60}, whereas the Li atoms initially placed closer to the C–C bond in the junction (Pos1 and Pos2@C_{60}) are repelled. This repositioning may be attributed to the strong covalent bond between graphene and C_{60}, which may prevent Li from forming bonds with carbon atoms in the system and keep Li out of the junction. The adsorption energies are also low near the graphene-C_{60} junction (region 2; −2.345 eV) and between C_{60}s (region 3; −2.158 eV) owing to the strong electron affinity of C_{60}. The amount of charge transfer from an adsorbed Li atom to the graphene-C_{60} nanobud system ranges from 0.785e to 0.871e depending on its position. The corresponding band structures of the one-Li-adsorbed nanobud systems, presented in Fig. 5, did not substantially change compared to the parent system prior to adsorption. However, the bands shift downward when the Li atom is adsorbed on the C_{60} side.

Adsorption of multiple Li atoms on the graphene-C_{60} nanobud system

To further investigate the adsorption mechanism, we added additional Li atoms at various sites in each region. Because the energy density is proportional to the number of Li atoms, it is very important to efficiently utilize the surface provided by the graphene-C_{60} electrode instead of forming Li–Li clusters. Moreover, the Li capacity can be maximized by covering each of the carbon rings in the graphene-C_{60} system with a Li atom. Systematic experiments were necessary to predict the adsorption direction on the nanobud system from the various adsorption sites. For this purpose, we provided a second Li atom with respect to the first Li atom with the lowest energy in each region of the nanobud system. However, there were various possibilities for determining the position of the second Li atom. Therefore, we defined the position of the second Li atom as the nearest-neighboring (N.N.) site or the next-nearest-neighboring (N.N.N.) site along the axis of the graphene surface on the graphene side. We also assumed that the second Li atom was adsorbed on the pentagonal or hexagonal ring on the C_{60} side in the radial or axial direction along the axis of the graphene to form the N.N. or N.N.N. configuration.

The initial and optimized structures of systems with two Li atoms adsorbed in different regions on the graphene-C_{60} nanobud system are displayed in Fig. 6. The Li adsorption energies of both Li atoms calculated using equation (1) are listed in Table 3. In region 1 of the nanobud system (Fig. 6a), two-Li adsorption results in the same adsorption energy using either the N.N.N. scheme (−1.971 eV) or the N.N. scheme (−1.972 eV). This is because both the second Li atoms moved to similar positions on the C_{60} side due to the strong electron affinity of C_{60}. Furthermore, the two-Li adsorption energy (−1.972 eV) was lower than that of the one-Li system (−1.905 eV), even though the adsorption energy usually increases as the number of Li atoms increases. This result is also related to the size of the unit structure because both Li atoms are strongly affected by the presence of C_{60}; therefore, the adsorption is even lower in the two-Li system. The adsorption energies were low and similar values were obtained for each position (Fig. 6b, −2.109 to −2.141 eV) in region 2 because of simultaneous interactions with both components. The adsorption energy in region 3 (between C_{60}s) was also low, ranging from −1.943 to −2.229 eV, because of the strong electron affinity of C_{60}. In regions 2 and 3 of the nanobud system, it appeared that the adsorption was independent of the adsorption sites when compared with the other regions, although the adsorption

energy of the N.N.N. scheme was slightly lower than the N.N. scheme in both regions. In region 4, the adsorption energy was calculated to be −1.987 eV for the pentagonal site (Fig. 6d, N.N.N. site) and −1.905 eV for the hexagonal site (N.N. site).

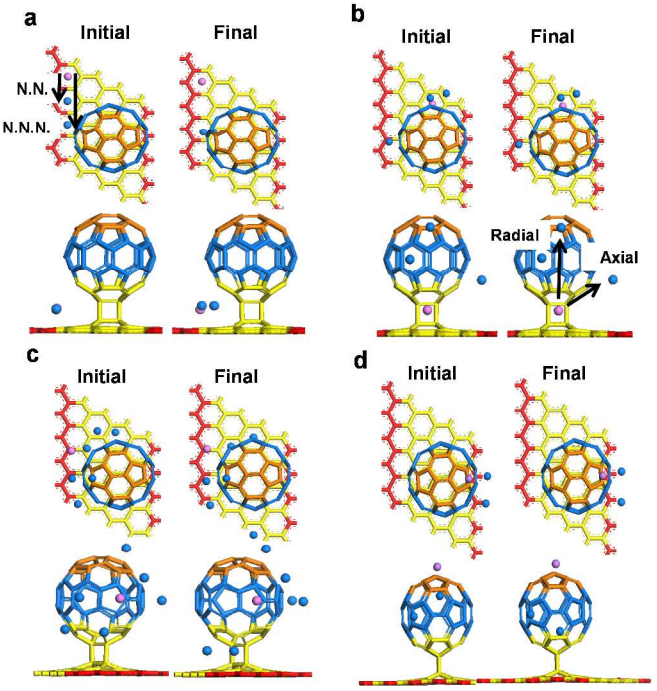

Fig. 6 The initial and optimized structures for the adsorption of two Li atoms on graphene-C_{60} nanobuds in different regions: (a) region 1, (b) region 2, (c) region 3, and (d) region 4 (1st Li atom: purple and 2nd Li atom: blue).

Table 3 Adsorption energies for the adsorption of two Li atoms on the graphene-C_{60} nanobud system

System	Adsorption Energy (eV)
2 Li on region1: N.N.N. site	−1.971
2 Li on region1: N.N. site	−1.972
2 Li on region2: Radial (N.N.N. site)	−2.141
2 Li on region2: Radial (N.N. site)	−2.133
2 Li on region2: Axial (N.N. site)	−2.109
2 Li on region3: Axial (N.N.N. site)	−2.130
2 Li on region3: Axial (N.N. site)	−2.091
2 Li on region3 to region2: N.N.N. site	−2.229
2 Li on region3 to region2: N.N. site	−2.199
2 Li on region3 to region4: N.N.N. site	−1.984
2 Li on region3 to region4: N.N. site	−1.943
2 Li on region4: Radial (N.N.N. site)	−1.987
2 Li on region4: Radial (N.N. site)	−1.905
18 Li atoms on graphene-C_{60} nanobud	−1.684

This result suggested a slight preference for Li adsorption via the N.N.N. scheme rather than the N.N scheme; however, this dependence was weak when we considered both the unit size of the system and the planar structure of the graphene. The Li adsorption mechanism was strongly influenced by C_{60}; therefore, Li adsorption will occur over the entire C_{60} surface before proceeding to the graphene sites in the graphene-C_{60} nanobud system. We also determined the corresponding changes in the band structures for several two-Li atom systems in each region of the graphene-C_{60} nanobud system, as shown in Fig. 7. Compared with the one-Li adsorption system, significant band shifts were observed whenever another Li atom was added to the nanobud system. The bands in close proximity to the additional Li atom were mainly affected and shifted down, owing to the increased in Fermi levels as electrons were injected from the Li atoms into the system.

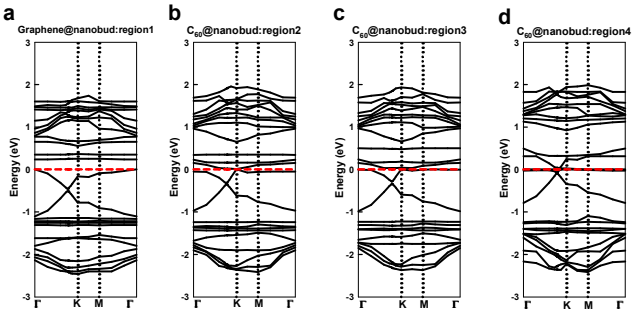

Fig. 7 Band structures for adsorption of two Li atoms in different regions on the graphene-C_{60} nanobud system: (a) region 1, (b) region 2, (c) region 3, and (d) region 4.

Finally, we added many Li atoms around the graphene-C_{60} nanobud system based on the N.N.N. scheme. The initial and optimized structures for the addition of 18 Li atoms on the substrate are presented in Fig. 8a, and the adsorption energy is listed in Table 3. In this scheme, the Li storage capability of the graphene-C_{60} nanobud system is increased by ~3 times and 1.5 times compared with the Li capability of the single graphene and C_{60} with the same volume (or area), respectively. From the optimized structure, it was clear that the Li atoms initially attached to the graphene-side sites were attracted toward the C_{60}. However, Li atoms initially located around C_{60} retained their positions.

The adsorption energy for the multi-Li adsorption was −1.684 eV for the entire nanobud system. This adsorption energy indicated that Li adsorption will take place on the C_{60} side until all of the available sites are completely filled before proceeding to the graphene sites, as found for the adsorption of two Li atoms. Even though the Li adsorption energy decreased with an increasing number of Li atoms, all of these adsorption energies are lower than the Li–Li binding energy (−1.030 eV).[14] Therefore, Li cluster formation is not likely to occur until all of the available sites on the graphene-C_{60} nanobud system are covered. In addition, the adsorption energy is lower than those of pure graphene (−1.086 eV) and C_{60} (−1.594 eV) systems with the same number of Li atoms. Therefore, in terms of Li adsorption, the graphene-C_{60} nanobud system appears to be promising for use as a possible electrode in Li batteries. Fig. 8b shows the band structure of the multi-Li adsorbed graphene-C_{60} nanobud system. The number of available energy bands around the Fermi level increased significantly, which indicated that Li adsorption enhanced the metallic characteristics of the system, such as its conductivity. This result was confirmed by the DOS, shown in Fig. 8c as a function of the number of Li atoms. In

this figure, the Li-adsorbed systems have more DOS around the Fermi level, especially when more than two Li atoms are adsorbed, compared with the graphene-C_{60} nanobud system prior to adsorption. This result demonstrates the enhanced metallic character of the graphene-C_{60} nanobud system, which could contribute to increases in its electron transport properties.

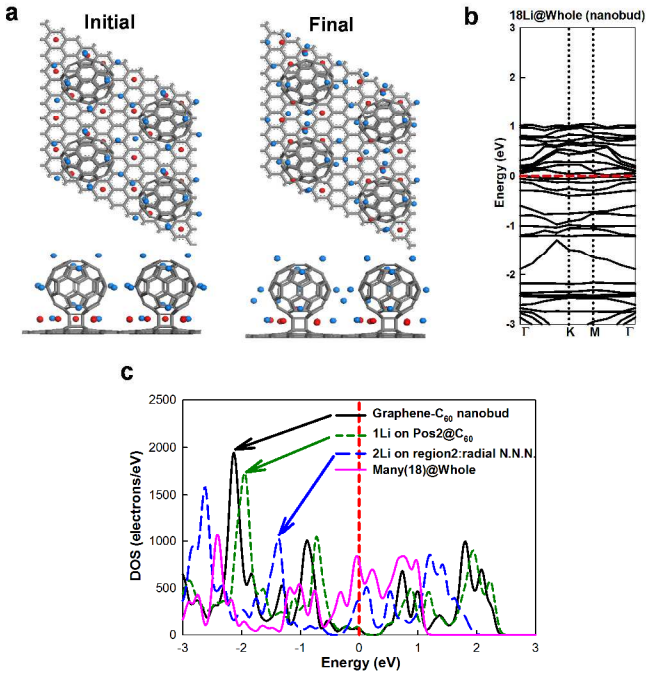

Fig. 8 (a) Initial and optimized structures, (b) band structure, and (c) density of states for the multi-Li adsorbed system.

Conclusions

We investigated Li adsorption on a graphene-C_{60} nanobud system using DFT. Although the hybrid system was found to retain the characteristics of its graphene and C_{60} components in its electronic structure, the covalently bonded graphene-C_{60} nanobud:hh system demonstrated charge transfer from graphene to C_{60} ($|0.059|e$). In contrast, a small band gap (0.30 eV) was observed for the graphene-C_{60} nanobud:hp system after the [2+2] cycloaddition reaction.

We found that Li adsorption was enhanced for the graphene-C_{60} nanobuds compared with pure graphene. This enhanced adsorption capability may be explained by the high electron affinity of C_{60} and the charge transfer from graphene to C_{60}. Furthermore, by analyzing the Li adsorption as a function of the regions in the graphene-C_{60} system, we determined that Li adsorption would preferentially occur on the C_{60} side, specifically at the space between graphene and C_{60} or between two C_{60}s, and proceed toward the graphene side. Consequently, it is unlikely that Li clusters would be formed in this system because the Li–C adsorptive interaction was more stable than the Li–Li binding interaction.

Although there was no significant change in the band structure after one Li atom was adsorbed on the graphene-C_{60} nanobud system, additional Li adsorptions shifted the energy bands downward and even removed the band gap of the nanobud system as a result of electron injection from Li to the system. The DOS in the nanobud system also indicated that the metallic character of the graphene-C_{60} system was enhanced as the number of Li atoms increased. Hence, it is expected that the graphene-C_{60} nanobud system will demonstrate enhanced conductive properties along with excellent Li adsorption capabilities compared with pure graphene.

Acknowledgements

This research was supported by the Basic Science Research Program through the National Research Foundation of Korea (NRF) funded by the Ministry of Science, ICT & Future Planning (2014R1A1A1004096). This research was supported by Global Frontier Program through the Global Frontier Hybrid Interface Materials (GFHIM) of the National Research Foundation of Korea (NRF) funded by the Ministry of Science, ICT & Future Planning (2013M3A6B1078881).

Notes and references

[a] School of Physics, Georgia Institute of Technology, 837 State Street, Atlanta, GA 30332-0430, USA.
[b] Department of Organic Material Science and Engineering, Pusan National University, 2, Busandaehak-ro 63beon-gil, Geumjeong-gu, Busan 609-735, Republic of Korea.
[c] Graduate School of EEWS, Korea Advanced Institute of Science and Technology, 291 Daehak-ro, Yuseong-gu, Daejeon 305-701, Republic of Korea.
[d] School of Materials Science and Engineering, Georgia Institute of Technology, 771 Ferst Drive NW, Atlanta, GA 30332-0245, USA.
* Corresponding authors: seunggeol.lee@pusan.ac.kr (S.G. Lee), Phone: +82-51-510-2412, Fax: +82-51-512-8175; SeungSoon.Jang@mse.gatech.edu (S.S. Jang), Phone: +1-404-385-3356, Fax: +1-404-894-9140

1 (a) Y. H. Liu, J. S. Xue, T. Zheng, J. R. Dahn, *Carbon* 1996, **34**, 193; (b) J. R. Dahn, T. Zheng, Y. Liu, J. S. Xue, *Science* 1995, **270**, 590.
2 S. M. Mukhopadhyay, *Nanoscale multifunctional materials : science and applications*, Wiley, Hoboken, N.J., 2012.
3 (a) M. Khantha, N. A. Cordero, L. M. Molina, J. A. Alonso, L. A. Girifalco, *Phys. Rev. B* 2004, **70**, 125422; (b) K. T. Chan, J. B. Neaton, M. L. Cohen, *Phys. Rev. B* 2008, **77**, 235430; (c) W. Q. Deng, X. Xu, W. A. Goddard, *Phys. Rev. Lett.* 2004, **92**, 166103; (d) H. Tachikawa, Y. Nagoya, T. Fukuzumi, *J. Power Sources* 2010, **195**, 6148; (e) K. Persson, Y. Hinuma, Y. S. Meng, A. Van der Ven, G. Ceder, *Phys. Rev. B* 2010, **82**, 125416; (f) G. Mpourmpakis, E. Tylianakis, G. E. Froudakis, *Nano Lett.* 2007, **7**, 1893; (g) C. Ataca, E. Akturk, S. Ciraci, H. Ustunel, *Appl. Phys. Lett.* 2008, **93**, 043123; (h) F. Valencia, A. H. Romero, F. Ancilotto, P. L. Silvestrelli, *J. Phys. Chem. B* 2006, **110**, 14832; (i) C. Uthaisar, V. Barone, J. E. Peralta, *J. Appl. Phys.* 2009, **106**, 113715.
4 (a) G. X. Wang, X. P. Shen, J. Yao, J. Park, *Carbon* 2009, **47**, 2049; (b) E. Yoo, J. Kim, E. Hosono, H. Zhou, T. Kudo, I. Honma, *Nano Lett.* 2008, **8**, 2277; (c) S. Stankovich, D. A. Dikin, G. H. B. Dommett, K. M. Kohlhaas, E. J. Zimney, E. A. Stach, R. D. Piner, S. T. Nguyen, R. S. Ruoff, *Nature* 2006, **442**, 282.
5 (a) X. J. Wu, X. C. Zeng, *Nano Lett.* 2009, **9**, 250; (b) S. Saito, A. Oshiyama, *Phys. Rev. B* 1994, **49**, 17413; (c) S. Patchkovskii, J. S. Tse, S. N. Yurchenko, L. Zhechkov, T. Heine, G. Seifert, *Proc. Natl. Acad. Sci. U. S. A.* 2005, **102**, 10439; (d) A. Kuc, L. Zhechkov, S. Patchkovskii, G. Seifert, T. Heine, *Nano Lett.* 2007, **7**, 1; (e) F. S. E. Skardi, M. D. Ganji, *Mater. Chem. Phys.* 2013, **142**, 44; (f) M. Wang, C. M. Li, *PCCP* 2011, **13**, 5945.
6 (a) V. Gupta, P. Scharff, K. Risch, H. Romanus, R. Muller, *Solid State Commun.* 2004, **131**, 153; (b) J. L. Delgado, P. de la Cruz,

A. Urbina, J. T. L. Navarrete, J. Casado, F. Langa, *Carbon* 2007, **45**, 2250; (c) X. Zhang, Y. Huang, Y. Wang, Y. Ma, Z. Liu, Y. Chen, *Carbon* 2009, **47**, 334; (d) M. Buttner, P. Reinke, *J. Phys. Chem. C* 2009, **113**, 8107.

7 (a) B. Delley, *J. Chem. Phys.* 1990, **92**, 508; (b) B. Delley, *J. Chem. Phys.* 2000, **113**, 7756.

8 J. P. Perdew, K. Burke, M. Ernzerhof, *Phys. Rev. Lett.* 1996, **77**, 3865.

9 (a) S. Kwon, J. I. Choi, S. G. Lee, S. S. Jang, *Comp Mater Sci* 2014, **95**, 181; (b) S. G. Lee, J. I. Choi, W. Koh, S. S. Jang, *Appl Clay Sci* 2013, **71**, 73; (c) S. Kwon, S. G. Lee, E. Chung, W. R. Lee, *Bull. Korean Chem. Soc.* 2015, **36**, 11.

10 (a) W. Koh, J. I. Choi, S. G. Lee, W. R. Lee, S. S. Jang, *Carbon* 2011, **49**, 286; (b) W. Koh, J. I. Choi, K. Donaher, S. G. Lee, S. S. Jang, *ACS Appl. Mater. Interfaces* 2011, **3**, 1186; (c) W. Koh, J. I. Choi, E. Jeong, S. G. Lee, S. S. Jang, *Curr. Appl. Phys.* 2014, **14**, 1748; (d) W. Koh, H. S. Moon, S. G. Lee, J. I. Choi, S. S. Jang, *Chemphyschem* 2015, **16**, 789.

11 S. Grimme, J. Antony, S. Ehrlich, H. Krieg, *J. Chem. Phys.* 2010, **132**, 154104.

12 U. Zimmermann, N. Malinowski, A. Burkhardt, T. P. Martin, *Carbon* 1995, **33**, 995.

13 Q. Sun, P. Jena, Q. Wang, M. Marquez, *J. Am. Chem. Soc.* 2006, **128**, 9741.

14 G. H. K.P. Huber, *Constants of Diatomic Molecules*, Van Nostrand Reinhold, New York, NY, 1979.